Chapter 3

In Situ X-ray Absorption Studies of Supported Manganese Oxide Catalysts During Ozone Decomposition

3.1 Introduction

With the widespread availability of synchrotron radiation sources and standardized data analysis software, X-ray absorption spectroscopy (XAS) has become a convenient technique for probing local structure in catalysts. Extended X-ray absorption fine structure (EXAFS) is used to determine the atomic distances and coordination numbers, while X-ray absorption near-edge structure (XANES) is used to study the electronic structure, oxidation state, and coordination chemistry (e.g., octahedral, tetrahedral coordination) of the absorbing atom [1, 2, 3].

The structure of 3 wt % manganese oxide catalysts supported on Al_2O_3, ZrO_2, TiO_2, and SiO_2 was studied using EXAFS and XANES measurements [4, 5]. In these studies analysis of the Mn K-edge EXAFS spectra indicated that the manganese active centers were surrounded by five oxygen atoms in all the supported catalysts and that the active centers were of a monomeric type for the Al_2O_3-supported catalyst and multinuclear for the other supports. Analysis of Mn L-edge spectra showed that there was a shift to lower energy in the position of the L_{II} and L_{III} edge features along with an increase in the intensity in the sequence $Al_2O_3 > ZrO_2 > TiO_2 > SiO_2$.

This implied that the density of empty d-states was the largest for the Al_2O_3-supported catalyst and the smallest for the SiO_2-supported catalyst. Brown et al. [6] studied a dispersed manganese dioxide catalyst (MnO_2-SiO_2) with EXAFS spectroscopy and concluded that the manganese active center was close to a +5 oxidation state.

The "white line", which is an intense feature within about 10 eV of the threshold, is due to the spectroscopic transition from 1s to p states for K-edge or 2p to d states for L-edge in XANES [7, 8]. The white line area in K-edge is directly related to the transition of a 1s core electron to a bound state such as an empty or partially filled molecular orbital [9]. An increase in white line area corresponds to an increase in the density of empty states capable of accepting an electron. It was reported that supported metal catalysts usually had somewhat more intense white lines than corresponding bulk metals [10]. Thus, the study of the white lines in the supported metal oxide catalysts will give better understanding of their structural properties.

The work presented in this chapter used *in situ* Mn K-edge XAS spectra to study the structural and electronic properties around manganese centers during the ozone decomposition reaction over MnO_x/SiO_2 and MnO_x/Al_2O_3 catalysts.

3.2 Experimental

3.2.1 Catalyst preparation

The manganese oxide catalysts used in this study were 3 and 10 wt % MnO_x/SiO_2 and 3 and 10 wt % MnO_x/Al_2O_3. The catalysts were prepared by the incipient wetness technique, using solutions of manganese acetate tetrahydrate, Mn $(CH_3COO)_2 \cdot 4H_2O$ (Aldrich, 99.99 %), in

distilled water. The supports were SiO_2 (Cabot, Cabosil LM130, 134 m^2 g^{-1}) and Al_2O_3 (Degussa, Aluminumoxid C, 96 m^2 g^{-1}), and were calcined at 773 K for 6 h before impregnation. After impregnation the materials were dried at 393 K for 6 h and then cooled and ground to ensure homogeneity. The samples were then calcined at 773 K for another 6 h at a heating rate of 0.83 K/s (5 K/min).

3.2.2 Catalyst characterization

X-ray diffraction (XRD) patterns, BET surface areas, and dispersion values of the catalyst samples were obtained the same way as described in Chapter 2.

Temperature-programmed reduction (TPR) and oxygen chemisorption measurements were carried out in the same system as before. Quantities of 0.2 g of catalysts were used in the experiments.

For the TPR measurements the catalyst was pretreated at 773 K for 2 h in 54 µmol/s (80 cm^3/min) of oxygen (Air Products, > 99.6 %) flow to remove excess moisture and carbon impurities. The catalyst sample was then reduced in 68 µmol/s (100 cm^3/min) of hydrogen (Air products, > 99.6 %) flow from room temperature to 1073 K at a rate of 0.03 K/s (2 K/min). The mass spectrometer signal of H_2O^+ (m/e =18) was monitored during the reduction process to determine the reduction temperature (T_{red}). For the 3 wt % samples, which were highly dispersed phase without bulk, the reduction temperature was taken after the first reduction peak. For the 10 wt % samples the reduction temperature was taken to be the temperature right before the onset of the bulk reduction as before. Oxygen chemisorption experiments were then performed at this reduction temperature with the same procedure mentioned in Chapter 2.

3.2.3 *In Situ* XAS (x-ray absorption spectroscopy) measurements

The *in situ* XAS measurements were carried out in transmission mode at the NSLS (National Synchrotron Light Source) using the X18B beam line with a 2.5 GeV ring energy and 300-400 mA ring current. The beam line used a Si (111) crystal monochromator and gave an energy resolution of 2 eV. Figure 3-1 shows the schematic of the *in situ* cell used for these measurements.

The reactor is a 2 cm diameter quartz tube capped with Kapton windows. The catalyst, after being pressed into a wafer of 0.1 cm thickness and 1.5 cm diameter, was placed in a quartz sample holder in the center of the reactor. Temperature was measured by a thermocouple placed directly above the sample wafer. A temperature controller (Cole Parmer Digi-Sense R/S) and a Ni-Cr heating element (Omega Engineering, Inc., PN NI80-025050 FT, NI80/CR20) wrapped around the reactor tube kept the reaction zone temperature within 2 K of the intended temperature throughout the experiments. The sample was pretreated at 473 K for 2 h in pure oxygen (Air products, > 99.6 %) before reaction. Ozone was generated by running pure oxygen (Air products, > 99.6 %) through a corona discharge in a high voltage ozone generator (Ozonelab^{TM} OL80) and the ozone concentration was measured by an ozone monitor (In USA, Model H1) equipped with a UV light detector.

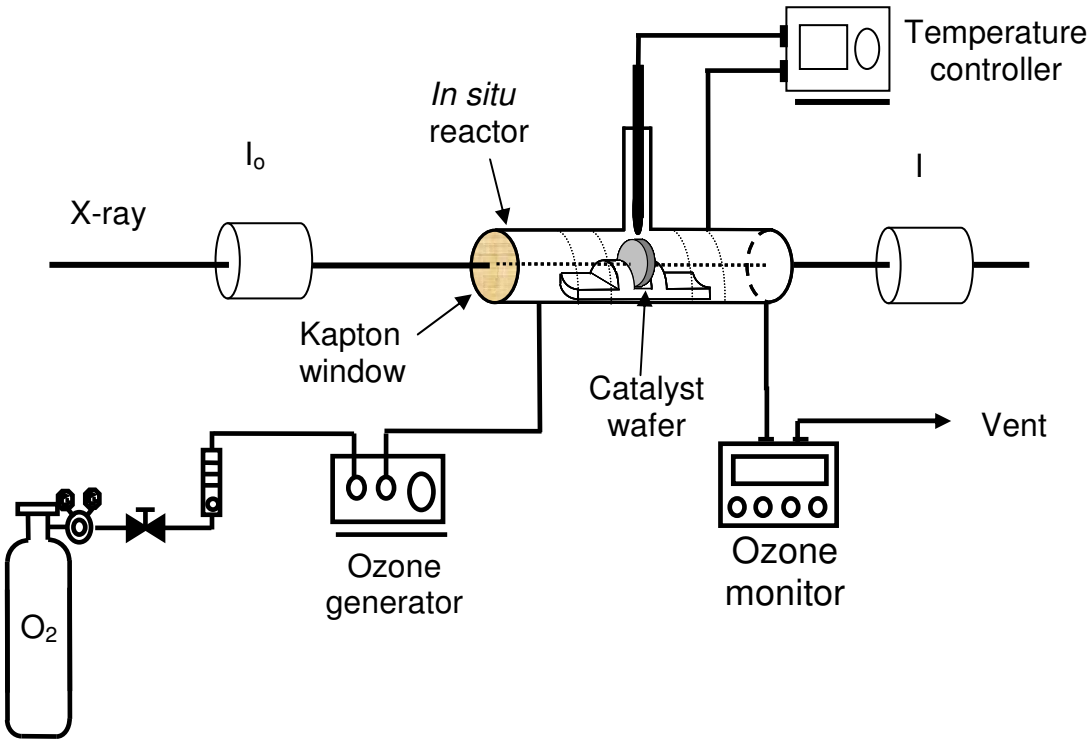

Figure 3-1. Schematic diagram of *In situ* X-ray absorption cell.

After pretreatment, the sample was maintained at 473 K with oxygen flow, and the x-ray absorption data were acquired. Measurements of XANES spectra used an energy scanning rate of 0.5 eV/s while measurements of EXAFS spectra used a rate of 1 eV/s. Data were taken successively at 373 K, 323 K, 373 K, and 473 K, with two scans at the same temperature averaged. Experiments with oxygen and ozone were carried out in sequence at each temperature, with a waiting period of 40 min between each set of conditions. The oxygen flow was maintained at 136 μmol/s (200 cm^3/min) by a rotometer for all experiments, and the ozone concentration for all ozone experiments was kept at 1.0 mol % (10,000 ppm). The XANES and EXAFS results were analyzed with WinXas 2.3 software. Amplitude and phase shift functions of the Mn K-edge EXAFS spectra for a MnO_2 reference were employed to quantify the structural

parameters from the EXAFS data [11]. The white line area was obtained by fitting an arctangent background to the entire edge-jump region followed by fitting a Gaussian curve to the first intense peak in the spectrum [3].

$$\text{Arctangent [12]:} \qquad f(x) = \frac{H}{\pi} \cdot \arctan\left(\frac{\pi}{W} \cdot (x - P)\right) + \frac{H}{2}, \tag{1}$$

$$\text{Gaussian [12]:} \qquad f(x) = H \cdot e^{-\left(\frac{(x-P)}{W}\right)^2}, \tag{2}$$

where H is the peak height, P is the peak position and W is the full width at half maximum (FWHM).

3.3 Results and discussion

3.3.1 Oxygen chemisorption and surface area measurement results

A recent in-depth characterization study using EXAFS and XANES [13] of MnO_x/SiO_2 showed that the manganese in 3 wt % MnO_x/SiO_2 was atomically dispersed with 6 Mn-O nearest-neighbor bonds, while in 10 wt % MnO_x/SiO_2 the manganese oxide formed clusters with an average coordination of 5 Mn-O bonds around each Mn center. As will be discussed, the EXAFS results in this study are in general agreement with these results.

The temperature-programmed reduction (TPR) results also fit this picture. Figure 3-2 shows the H_2O^+ (m/e = 18) TPR traces for the 3 and 10 wt % MnO_x/SiO_2 and 3 and 10 wt % MnO_x/Al_2O_3 samples. The reduction profile of the 3 wt % MnO_x/SiO_2 sample (Figure 3-2a) shows a single feature at around 550 K consistent with the presence of a dispersed phase. The

profile for the 10 wt % MnO_x/SiO_2 sample (Figure 3-2b) shows a second peak at 635 K consistent with the formation of clusters. The profile for the 3 wt % MnO_x/Al_2O_3 sample (Figure 3-2c) shows a reduction features at around 560 K also indicating the presence of a dispersed phase and the profile for the 10 wt % MnO_x/Al_2O_3 sample (Figure 3-2d) shows a second peak at 635 K again indicating the existence of clusters. For the 3 wt % MnO_x/SiO_2 and 3 wt % MnO_x/Al_2O_3 samples, which were highly dispersed phase without bulk, the reduction temperature was taken after the first reduction peak, T_{red} = 613 K, for both samples. For the 10 wt % MnO_x/SiO_2 and 10 wt % MnO_x/Al_2O_3 samples the reduction temperatures were taken right before the onset of the bulk reduction, T_{red} = 500 K and T_{red} =480 K, respectively.

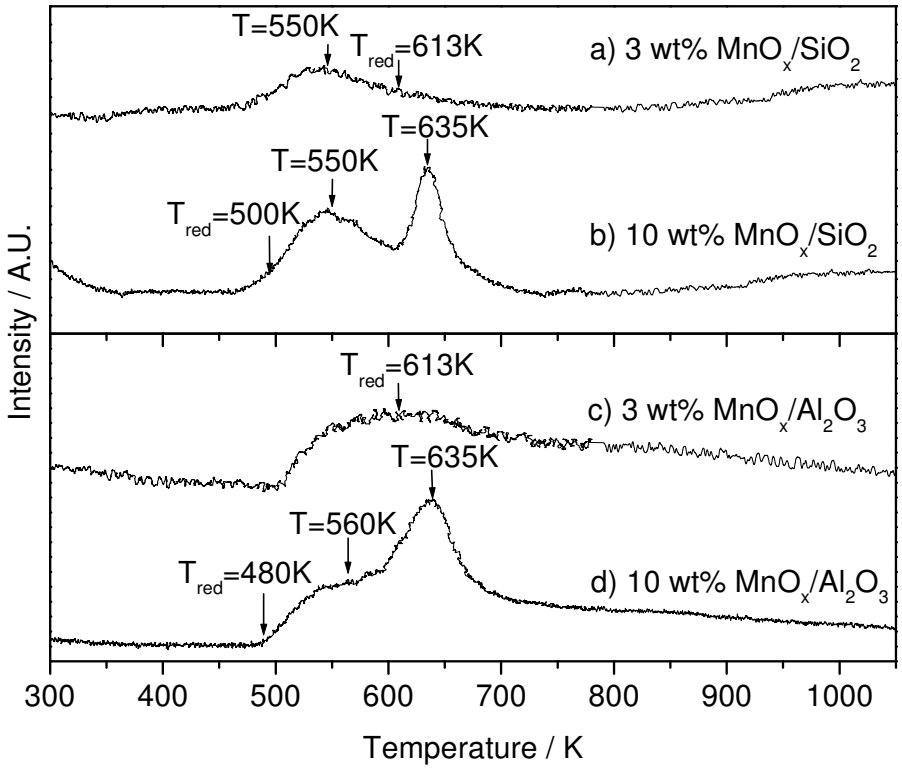

Figure 3-2. TPR traces for: a) 3 wt % MnO_x/SiO_2, b) 10 wt % MnO_x/SiO_2, c) 3 wt % MnO_x/Al_2O_3, and d) 10 wt % MnO_x/Al_2O_3.

The surface areas for the samples and the supports together with the oxygen uptake values and the dispersions were shown in Table 3-1. The dispersion decreases with increased loading, and is the smallest for the 10 wt % MnO_x/Al_2O_3 sample.

Table 3-1. Surface area, oxygen chemisorption, and dispersion values.

Catalyst	T_{red} K	S. A. $m^2\ g^{-1}$	O_2 Uptake $\mu mol\ g^{-1}$	Dispersion %
3 wt% MnO_x/SiO_2	613	120	150	91
10 wt% MnO_x/SiO_2	500	110	51	9.3
3 wt% MnO_x/Al_2O_3	613	92	120	73
10 wt% MnO_x/Al_2O_3	480	85	49	8.9
SiO_2	-	130	-	
Al_2O_3	-	96	-	

3.3.2 *In Situ* XAS and reactivity study

Figure 3-3 shows the Fourier transforms of the Mn K-edge *in situ* EXAFS spectra for the 3 wt % MnO_x/SiO_2 sample at 323 K, 373K, and 473 K with and without ozone. There is a broad peak at around 0.15 nm corresponding to a Mn-O bond and a small peak at around 0.23 nm corresponding to a Mn-Mn distance. The intensity of these peaks increases with the presence of ozone in all cases. Figure 3-4 displays the Fourier transforms for the 10 wt % MnO_x/SiO_2 sample and shows two peaks at around 0.15 nm and 0.23 nm for the Mn-O and Mn-Mn bonds, respectively. For this higher loading sample, however, there appears another large peak at around 0.32 nm due to the contributions of higher order shells in the larger particles. The larger particle sizes are consistent with the smaller dispersion value obtained from the oxygen chemisorption experiments.

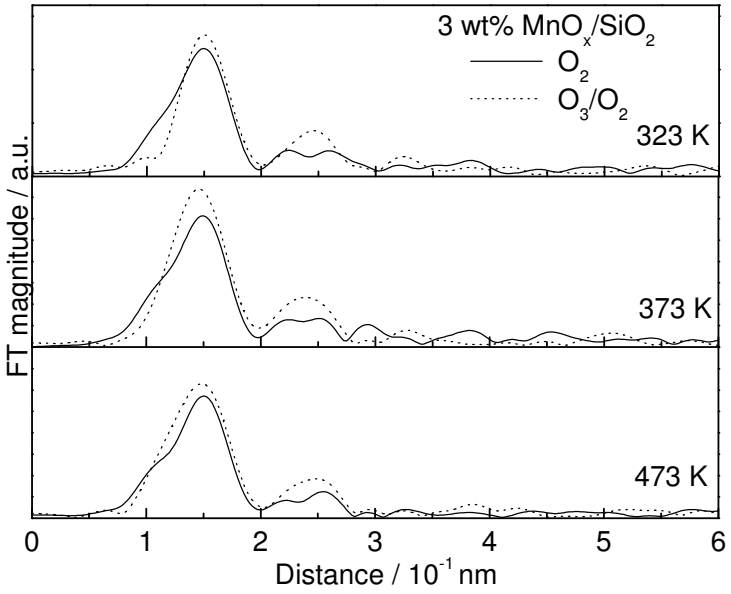

Figure 3-3. Fourier transforms of the Mn K-edge EXAFS spectra for 3 wt % MnO_x/SiO_2 catalyst at 323 K, 373 K, and 473 K with and without the presence of ozone. F_{tot} = 136 µmol/s (200 cm^3/min), ozone concentration = 10,000 ppm.

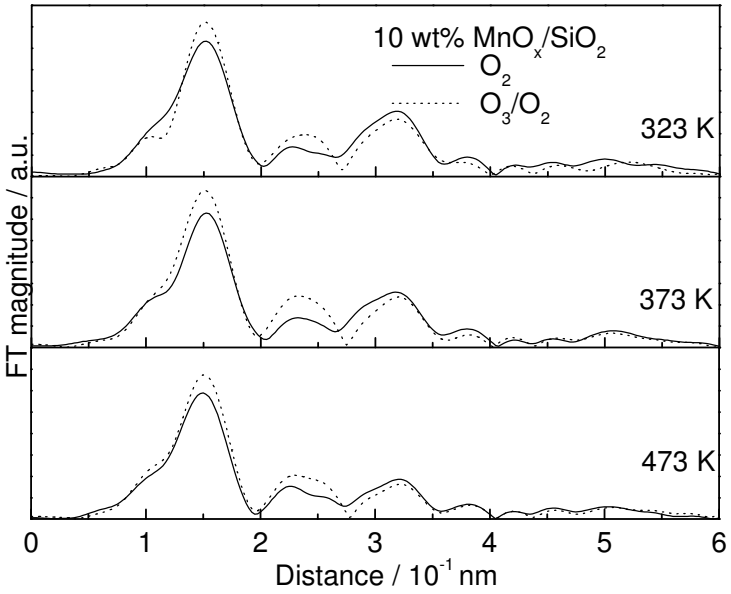

Figure 3-4. Fourier transforms of the Mn K-edge EXAFS spectra for 10 wt % MnO_x/SiO_2 catalyst at 323 K, 373 K, and 473 K with and without the presence of ozone. F_{tot} = 136 µmol/s (200 cm^3/min), ozone concentration = 10,000 ppm.

Figures 3-5 and 3-6 show the Fourier transforms of the Mn K-edge EXAFS spectra for the alumina-supported samples. As for the 10 wt % MnO_x/SiO_2 sample, three broad peaks (Figure 3-5 and Figure 3-6) appear at around 0.15 nm, 0.23 nm, and 0.32 nm due to the Mn-O, Mn-Mn, and higher order Mn-Mn and Mn-O shells, respectively. Unlike the case of the silica-supported samples, there was little increase in the intensity of the Mn-O bond in the presence of ozone. Similar to the silica-supported samples, the EXAFS results for the 10 wt % MnO_x/Al_2O_3 sample gave higher intensity for the higher order shells at around 0.32 nm, indicating the formation of larger particles.

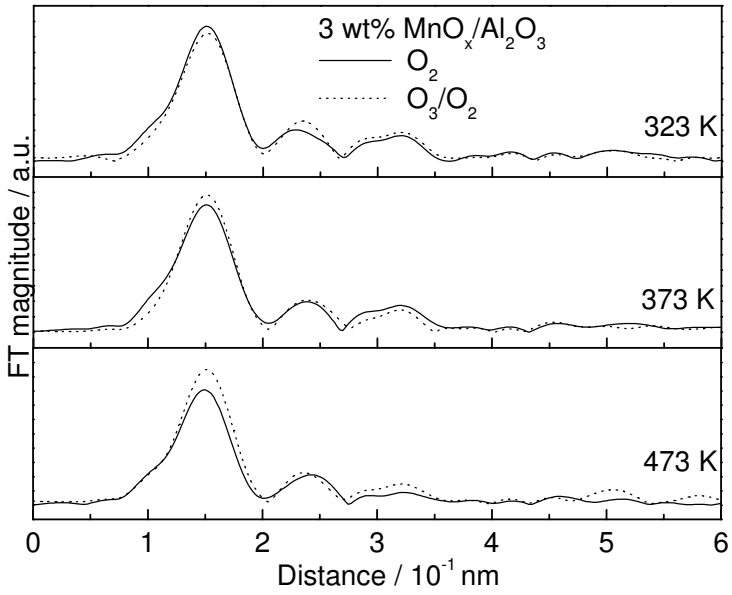

Figure 3-5. Fourier transforms of the Mn K-edge EXAFS spectra for 3 wt % MnO_x/Al_2O_3 catalyst at 323 K, 373 K, and 473 K with and without the presence of ozone. F_{tot} = 136 μmol/s (200 cm^3/min), ozone concentration = 10,000 ppm.

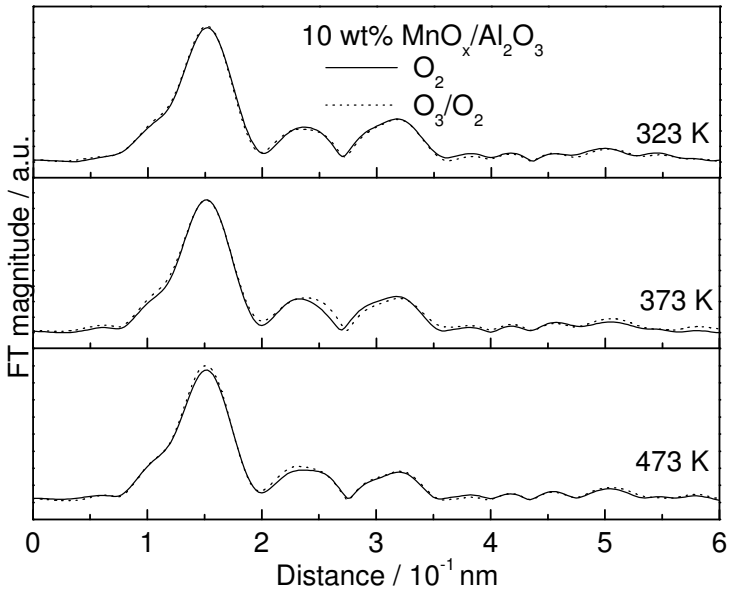

Figure 3-6. Fourier transforms of the Mn K-edge EXAFS spectra for 10 wt % MnO_x/Al_2O_3 catalyst at 323 K, 373 K, and 473 K with and without the presence of ozone. F_{tot} = 136 μmol/s (200 cm^3/min), ozone concentration = 10,000 ppm.

Curve fitting results for the Mn-O bond of these samples are presented in Tables 3-2 and 3-3. Also shown in the tables are the Mn-O bond distance (r), Debye-Waller factor (σ^2), energy shift (ΔE), and residual factor (R), which describes the quality of the fit. Upon exposure to ozone, an increase in the Mn-O coordination number and a decrease in the Mn-O bond distance at temperatures of 323 K, 373 K, and 473 K were obtained, which indicates that the oxidation state of manganese increased during the ozone decomposition reaction. In the lower loading 3 wt % MnO_x/SiO_2 sample the Mn-O coordination numbers are larger and the bond distances are smaller than those in the 10 wt % MnO_x/SiO_2 sample at the same reaction conditions. This indicates a higher oxidation state for the lower loading sample (Table 3-2) and is consistent with the results from our previous work [13]. For the alumina-supported samples, however, there are

no obvious changes in the coordination number or the bond distance of Mn-O with and without ozone, which indicates there is no further oxidation of the manganese with exposure to ozone (Table 3-3). For the silica-supported samples, in an oxygen atmosphere the Mn-O coordination numbers are close to 5 which is similar to the result obtained in our previous work [5]. In the presence of ozone the coordination numbers are close to 7 for the 3 wt % sample and to 6 for the 10 wt % sample. The rise in coordination numbers is reasonable. The 3 wt % MnO_x/SiO_2 sample has a structure close to octahedral and upon exposure to ozone the coordination increased to 7 with the formation of a peroxide species (Figure 3-7). The 10 wt % MnO_x/SiO_2 sample contains clusters of manganese oxide with a structure resembling a building block of Mn_3O_4, and with exposure to ozone the average coordination of this unit rises to 6 (Figure 3-8). For the alumina-supported samples, the Mn-O coordination numbers are close to 7 at all conditions may have a pentagonal bipyramid structure for the center manganese atom (Figure 3-9). This seven-coordinated manganese (II) structure was discussed in literature [14] for a Mn complex with a water molecule and a chlorine atom in the axial positions and four donor atoms (two nitrogens and two oxygens) of 2-aminobenzoylhydrazone and a second water molecule in the equatorial plane.

Table 3-2. EXAFS curve fitting results of the first shell Mn-O bond for the 3 wt % MnO_x/SiO_2 and 10 wt % MnO_x/SiO_2 samples.

Reaction condition	3 wt % MnO_x/SiO_2					10 wt % MnO_x/SiO_2				
	N	r nm	σ^2	ΔE keV	R %	N	r nm	σ^2	ΔE keV	R %
323 K, O_2	5.45	0.1909	0.0027	-4.31	1.48	5.26	0.1922	0.0017	-4.57	1.76
323 K, O_3/O_2	5.73	0.1910	0.0022	-3.48	3.67	5.39	0.1923	0.00099	-2.94	2.09
373 K, O_2	5.44	0.1905	0.0025	-4.22	1.25	4.96	0.1927	0.0014	-4.13	1.51
373 K, O_3/O_2	6.99	0.1893	0.0032	-4.52	2.04	6.12	0.1915	0.0020	-3.62	1.21
473 K, O_2	5.12	0.1909	0.0027	-3.78	1.16	4.78	0.1913	0.0017	-5.59	1.29
473 K, O_3/O_2	6.58	0.1901	0.0039	-3.60	2.04	6.48	0.1911	0.0032	-4.22	0.87

Table 3-3. EXAFS curve fitting results of the first shell Mn-O bond for the 3 wt % MnO_x/Al_2O_3 and 10 wt % MnO_x/Al_2O_3 samples.

Reaction condition	3 wt % MnO_x/Al_2O_3					10 wt % MnO_x/Al_2O_3				
	N	r nm	σ^2	ΔE keV	R %	N	r nm	σ^2	ΔE keV	R %
323 K, O_2	7.23	0.1914	0.0018	-3.66	1.71	7.17	0.1917	0.0018	-3.14	1.49
323 K, O_3/O_2	7.32	0.1913	0.0024	-3.02	1.65	7.22	0.1914	0.0018	-3.13	1.35
373 K, O_2	7.30	0.1913	0.0024	-3.24	1.75	7.06	0.1916	0.0017	-3.33	1.47
373 K, O_3/O_2	7.35	0.1912	0.0018	-3.08	1.76	7.13	0.1915	0.0022	-3.15	1.46
473 K, O_2	7.35	0.1907	0.0013	-4.35	0.46	6.71	0.1916	0.0023	-3.24	1.24
473 K, O_3/O_2	7.38	0.1905	0.0027	-3.69	1.34	6.84	0.1914	0.0022	-3.23	1.15

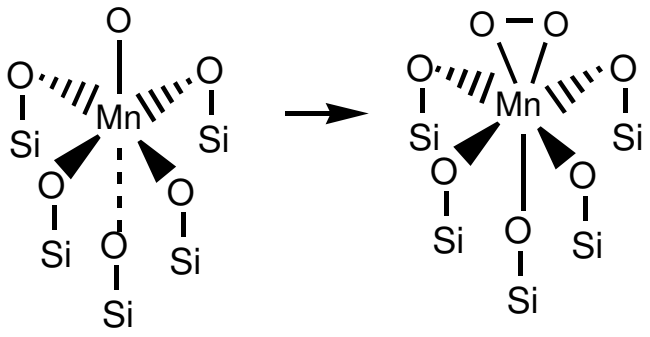

Figure 3-7. Manganese center structure change for the 3 wt % MnO_x/SiO_2 sample with exposure to ozone.

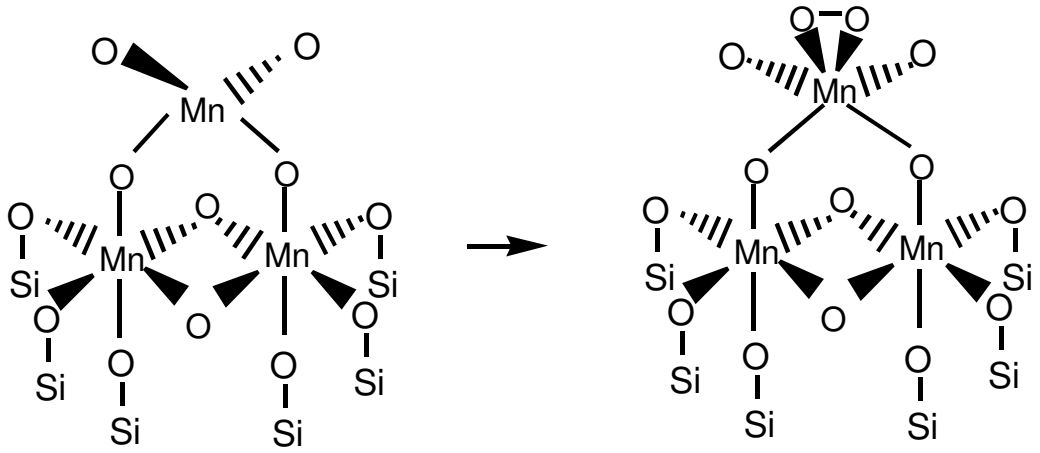

Figure 3-8. Manganese center structure change for the 10 wt % MnO_x/SiO_2 sample with exposure to ozone.

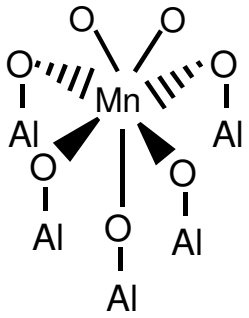

Figure 3-9. Manganese center structure for the 3 wt % MnO_x/Al_2O_3 and 10 wt % MnO_x/Al_2O_3 with and without exposure to ozone.

Figures 3-10, 3-11, 3-12, and 3-13 present the *in situ* Mn K-edge XANES and the white line calculation fitting results for the four catalysts. For the 3 wt % MnO_x/SiO_2 sample, the white line peaks are shifted to higher energy from 6.559 keV without ozone to 6.561 keV with ozone (Figure 3-10a). Similar behavior is observed for the 10 wt % MnO_x/SiO_2 catalyst, with the white line peaks being shifted from 6.559 keV without ozone to 6.560 keV with ozone (Figure 3-11a). This indicates that the samples are more oxidized with exposure to ozone. For the alumina-supported samples a similar shift of the white line peaks from 6.560 keV without ozone to a slightly higher energy with ozone is observed for the 3 wt % MnO_x/Al_2O_3 sample (Figure 3-12a), but nearly no shift for the 10 wt % MnO_x/Al_2O_3 sample is observed (Figure 3-13a).

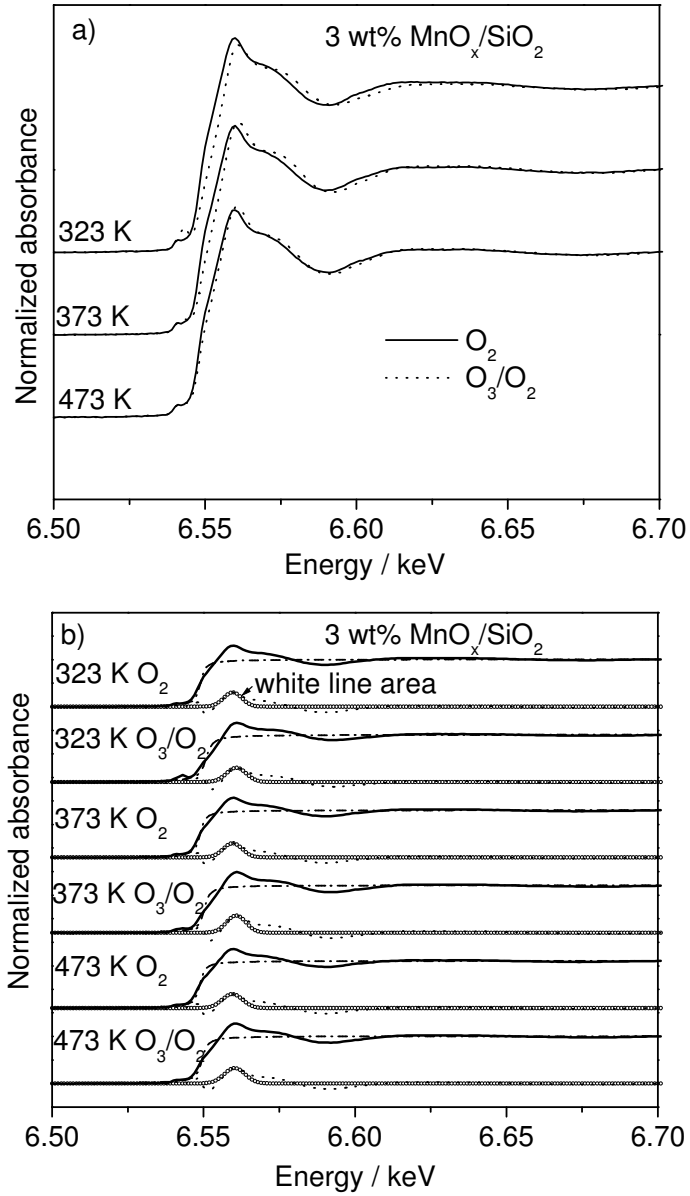

Figure 3-10. a) Mn K-edge XANES spectra for 3 wt % MnO_x/SiO_2 catalyst at 323 K, 373 K and 473 K with and without the presence of ozone. F_{tot} = 136 µmol/s (200 cm^3/min), ozone concentration = 10,000 ppm; and b) white line area calculation fitting for the corresponding spectra: (solid line —) XANES spectrum; (dash dot line -·-·) arctangent function; (dot line ····) subtraction of arctangent function from the XANES spectrum; (circle ○) Gaussian fitting.

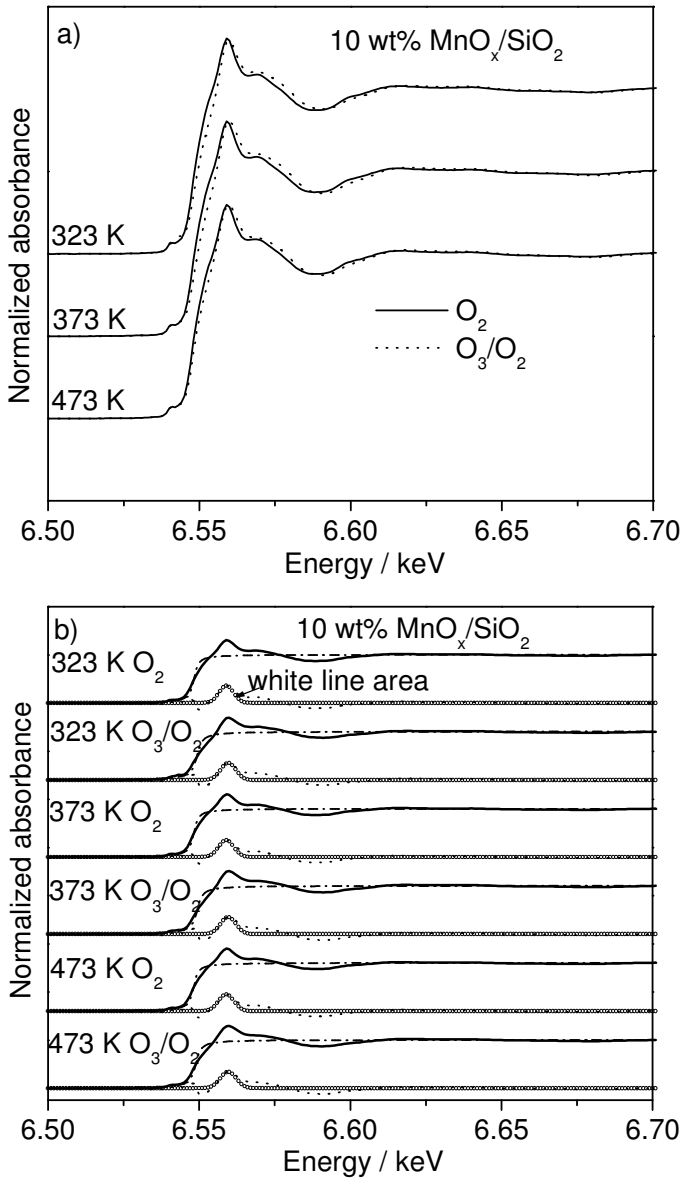

Figure 3-11. a) Mn K-edge XANES spectra for 10 wt % MnO_x/SiO_2 catalyst at 323 K, 373 K and 473 K with and without the presence of ozone. F_{tot} = 136 μmol/s (200 cm^3/min), ozone concentration = 10,000 ppm; and b) white line area calculation fitting for the corresponding spectra: (solid line —) XANES spectrum; (dash dot line -·-·) arctangent function; (dot line ····) subtraction of arctangent function from the XANES spectrum; (circle ○) Gaussian fitting.

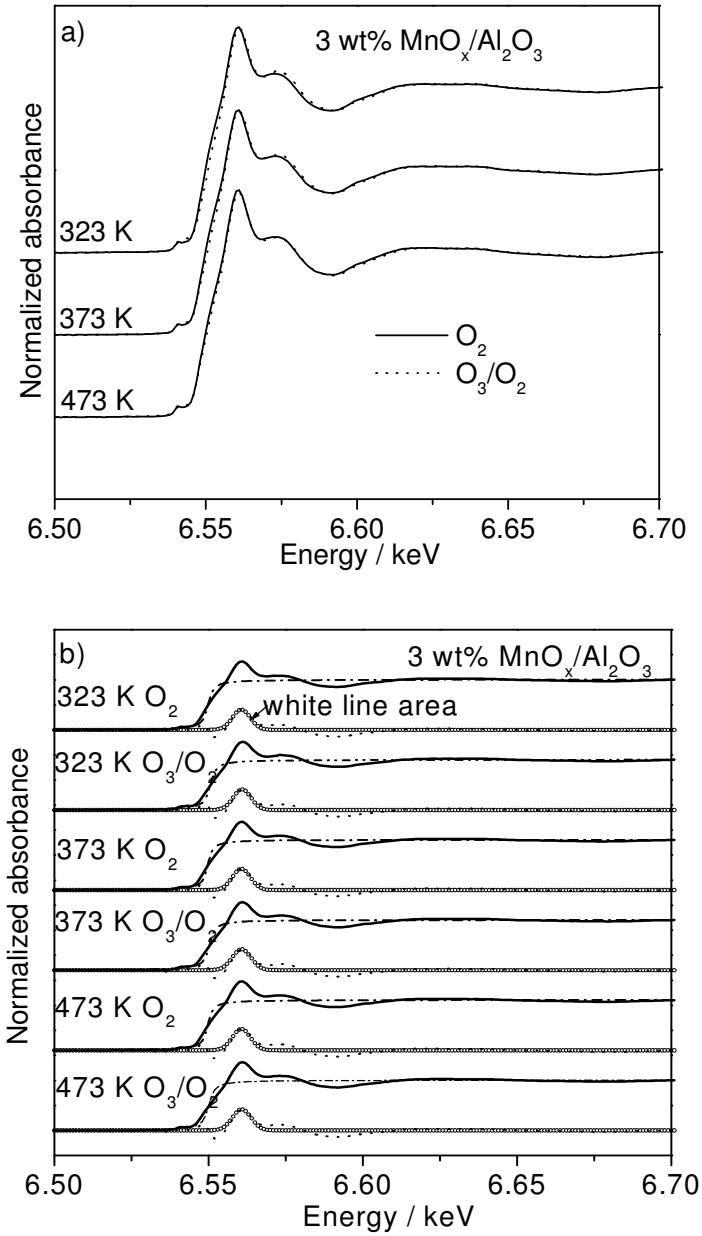

Figure 3-12. a) Mn K-edge XANES spectra for 3 wt % MnO_x/ Al_2O_3 catalyst at 323 K, 373 K and 473 K with and without the presence of ozone. F_{tot} = 136 µmol/s (200 cm^3/min), ozone concentration = 10,000 ppm; and b) white line area calculation fitting for the corresponding spectra: (solid line —) XANES spectrum; (dash dot line -·-·) arctangent function; (dot line ····) subtraction of arctangent function from the XANES spectrum; (circle ○) Gaussian fitting.

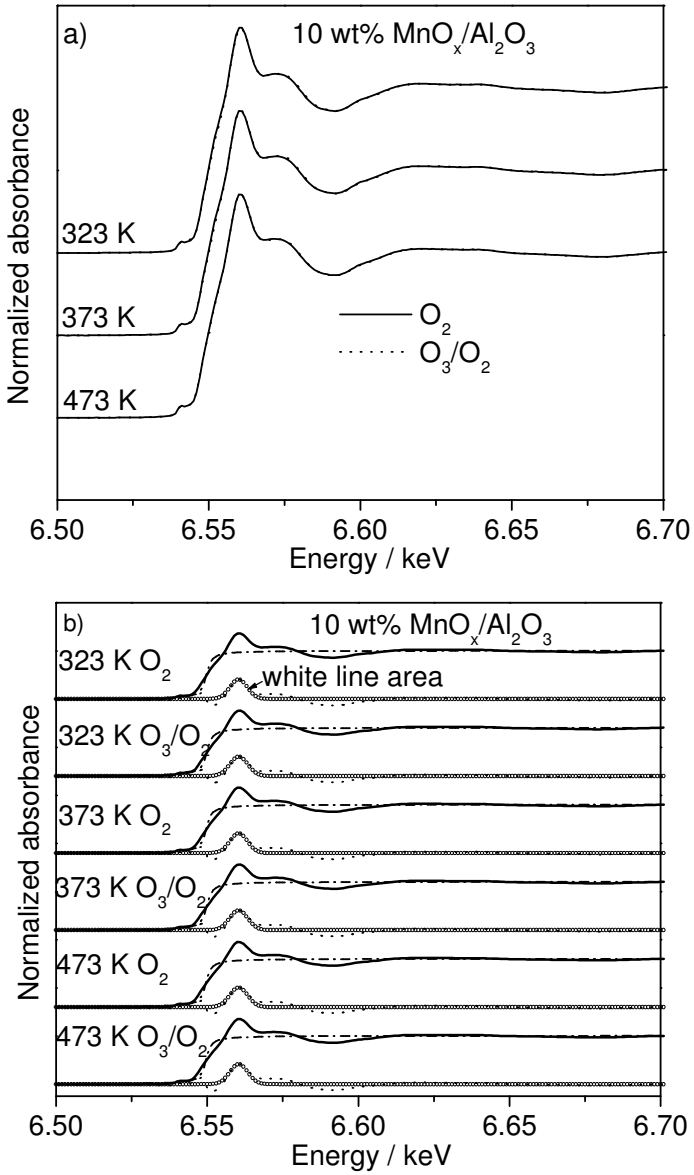

Figure 3-13. a) Mn K-edge XANES spectra for 10 wt % MnO_x/ Al_2O_3 catalyst at 323 K, 373 K and 473 K with and without the presence of ozone. F_{tot} = 136 µmol/s (200 cm^3/min), ozone concentration = 10,000 ppm; and b) white line area calculation fitting for the corresponding spectra: (solid line —) XANES spectrum; (dash dot line -·-·) arctangent function; (dot line ····) subtraction of arctangent function from the XANES spectrum; (circle ○) Gaussian fitting.

The absorption edge energy (E_0) and white line areas for the four different catalyst samples under different reaction conditions are shown in Tables 3-4 and 3-5. At each temperature, for both the 3 wt % and 10 wt % silica-supported samples E_0 is shifted to the higher energy region and the white line area increased with the presence of ozone (Table 3-4), while for both alumina-supported samples E_0 is not shifted but the white line area increased in the presence of ozone at each temperature (Table 3-5). Under the same reaction conditions, the lower loading sample has a larger white line area than the higher loading sample for both silica- and alumina-supported catalysts, indicating a higher oxidation state in the smaller particles.

Table 3-4. Calculated absorption edge (E_0) position and white line area results for the 3 wt % MnO_x/SiO_2 and 10 wt % MnO_x/SiO_2 samples.

Condition	3 wt% MnO_x/SiO_2		10 wt% MnO_x/SiO_2	
	Edge position keV	White line area keV ($\times 10^{-3}$)	Edge position keV	White line area keV ($\times 10^{-3}$)
323 K, O_2	6.549	2.273	6.548	2.146
323 K, O_3/O_2	6.551	2.455	6.549	2.222
373 K, O_2	6.549	2.313	6.548	2.193
373 K, O_3/O_2	6.551	2.684	6.549	2.249
473 K, O_2	6.549	2.485	6.548	2.237
473 K, O_3/O_2	6.551	2.808	6.549	2.256

Table 3-5. Calculated absorption edge (E_0) position and white line area results for the 3 wt % MnO_x/Al_2O_3 and 10 wt % MnO_x/Al_2O_3 samples.

Condition	3 wt% MnO_x/Al_2O_3		10 wt% MnO_x/Al_2O_3	
	Edge position keV	White line area keV ($\times 10^{-3}$)	Edge position keV	White line area keV ($\times 10^{-3}$)
323 K, O_2	6.550	2.958	6.550	2.925
323 K, O_3/O_2	6.550	2.981	6.550	3.004
373 K, O_2	6.550	3.132	6.550	2.955
373 K, O_3/O_2	6.550	3.201	6.550	3.087
473 K, O_2	6.550	3.148	6.550	3.037
473 K, O_3/O_2	6.550	3.212	6.550	3.091

Figure 3-14 presents the effect of temperature on the ozone decomposition conversion and the turnover frequencies (TOFs) for the silica- and alumina-supported catalysts. The TOFs were calculated for ozone decomposition conversion using the oxygen uptake values from the oxygen chemisorption experiments and the conversion values. It is evident that with the same loading the alumina-supported catalysts are more active than the silica-supported catalysts with higher TOFs (Figure 3-14b), while with the same support the higher loading 10 wt % catalysts are more active than the 3 wt % catalysts with higher TOFs (Figure 3-14)

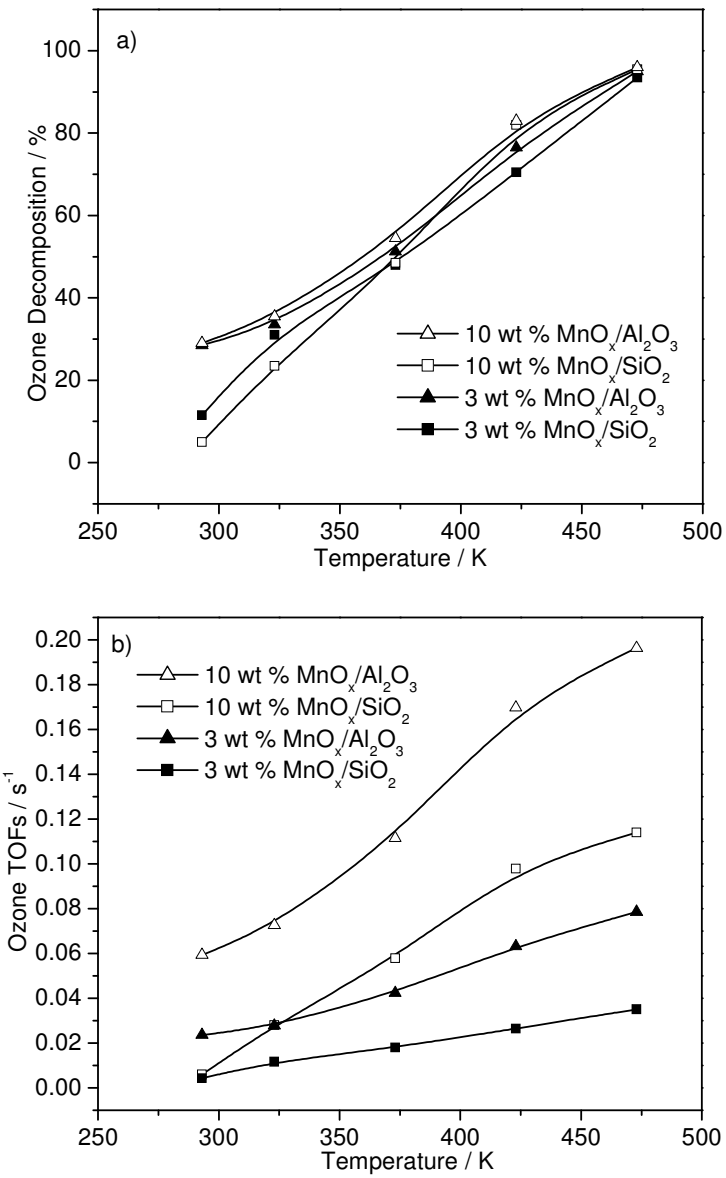

Figure 3-14. a) Ozone decomposition conversion and b) TOFs versus temperature for (▲) 3 wt % MnO_x/Al_2O_3, (Δ) 10 wt % MnO_x/Al_2O_3, (■) 3 wt % MnO_x/SiO_2, and (□) 10 wt % MnO_x/SiO_2 catalysts. F_{tot} = 136 μmol/s (200 cm^3/min), ozone concentration = 10,000 ppm.

The differences in the activity for catalyst samples with different supports and loadings can be well understood through their *in situ* XAS results. Supports have been found to have considerable effect on the activity of oxidation catalysts, for example, in the case of Mo and V oxide catalysts [15, 16, 17]. In methanol oxidation, Briand et al. [18] concluded that the specific activity was independent of the Mo structure, but was correlated to the nature of the oxide support. They found that the specific activity of the catalysts decreased in the order: ZrO_2 > MnO_2 > TiO_2 > Nb_2O_5 > Cr_2O_3 > Al_2O_3 > SiO_2, which coincided with the decreasing electronegativity of the metal cations. Burcham et al. [17] reported an identical trend in the reactivity of supported vanadium catalysts with Al_2O_3 being more electronnegative than SiO_2. Oyama et al. [19] found a similar activity trend in their study of methanol oxidation on titania-, alumina-, and silica-supported Mo catalysts, and explained this as being due to an electronic effect. They investigated the Mo L-edge NEXAFS spectra of the catalysts and found that the preexponential factors of the rate constants correlated with the Mo white line areas, which decreased in the order TiO_2 > Al_2O_3 > SiO_2. They also demonstrated that the order in preexponential factors depended on trends in the electronic partition function. Since the electronic partition function represents the ability of the metal centers to accept electrons, the origin of the activity changes could be related to the reducibility of the metal centers and is therefore an electronic effect.

In this study, the Mn K-edge white line areas for the alumina-supported samples were found to be larger than those of the silica-supported samples. It was proposed in the previous study [20, 21] that the mechanism of ozone decomposition is as follows:

$$O_3 + * \rightarrow O_2 + O* \qquad (3)$$

$$O_3 + O^* \rightarrow O_2 + O_2^* \quad (4)$$

$$O_2^* \rightarrow O_2 + * \quad (5)$$

where the third step, the decomposition of a peroxide intermediate to form molecular oxygen, was viewed as a slow step. In this step, the Mn center accepts electrons from the peroxide species and is reduced. Since this is an electron transfer process the rate of this step would be enhanced by an increased ability of the manganese center to accept electrons. A measure of this ability is given by the white line area in the XANES spectra of the samples, which is proportional to the density of states of unoccupied electronic levels. The white line areas for the alumina-supported catalyst were larger than those of the silica-supported catalysts, which indicate a higher electron-accepting ability for the alumina-supported catalysts. Thus this can explain their higher activity.

For the samples of the same support, there is a decrease in the white line area (Table 4 and Table 5) and the Mn-O coordination number with increasing loading (Table 6 and Table 7), which indicate a decrease in the oxidation state. However, the activity increased with increasing loading or decreasing oxidation state for the samples of the same support. This can be explained that for the same support because the oxidation state of the clusters is lower they can interact with ozone more readily to form the peroxide species (O_2^{2-}) and therefore the Mn atoms in the clusters become more positively charged. A similar trend was found in another work done by our lab where the loading effect was studied for 3 and 10 wt % silica-supported catalysts in the oxidation of acetone with the existence of ozone [13]. It was found that the 10 wt % catalyst was more active than the 3 wt % one with higher TOFs both for acetone and ozone conversion.

3.4 Conclusions

Manganese oxide catalysts (3 and 10 wt %) supported on SiO_2 and Al_2O_3 prepared through the incipient wetness impregnation method were studied using *in situ* x-ray absorption spectroscopy. The number of surface active sites was determined through oxygen chemisorption measurements at reduction temperatures of T_{red} = 613 K for the 3 wt % silica- and alumina-supported samples, T_{red} = 500 K and T_{red} = 480 K for the 10 wt % silica- and alumina-supported samples, respectively. There were two different reduction peaks for the 10 wt % catalyst samples for both supports indicating the formation of clusters, and one reduction peak for the 3 wt % samples due to the presence of a dispersed phase. For the silica-supported catalysts the x-ray absorption results showed that the ozone decomposition reaction gave rise to an apparent shift of the absorption edge energy (E_0) position to higher energy with the Mn-O coordination number of Mn increasing. For the alumina-supported samples, however, there was only a slight increase in the E_0 position for the 3 wt % sample and nearly no change for the 10 wt % sample with the coordination number of Mn-O being barely increased. For both supports, the intensity of the Mn-Mn bond increased with increasing loading indicating a lower dispersion. For the silica-supported samples, the Mn-O coordination number increased and the bond distance decreased with exposure to ozone, while for the alumina-supported samples there were no major changes for the coordination number and bond distance. Alumina-supported catalysts are more active than the silica-supported catalysts due to a higher electron-accepting ability for the alumina-supported catalysts. While, for the samples of same support, the higher loading sample was more active than the lower loading sample due to the lower oxidation state of the clusters and the Mn atoms in the clusters are more positively charged.

References:

(1) E. P. Bertin, *Principles and Practice of X-ray spectrometric Analysis*, Plenum press: New York, **1970**.

(2) B. K. Teo, D. C. Joy, *EXAFS Spectroscopy Techniques and Applications*, Plenum Press: New York, **1981**.

(3) J. Stöhr, *NXAFS Spectroscopy*, Springer Series in Surface Science, Springer: New York, **1992**, 25.

(4) R. Radhakrishnan, S. T. Oyama, Y. Ohminami, K. Asakura, *J. Phys. Chem. B*, **2001**, 105, 9067.

(5) R. Radhakrishnan, S. T. Oyama, J. G. Chen, K. Asakura, *J. Phys. Chem. B*, **2001**, 105, 4245.

(6) N. M. D. Brown, J. B. Mcmonagle, G. N. Greaves, *J. Chem. Soc., Faraday Trans*. 1, **1984**, 80, 589.

(7) D. C. Koningsberger, R. Prins, *X-Ray Absorption: Principle, Applications, Techniques of EXAFS, SEXAFS and XANES*, John Wiley & Son, New York, **1988**.

(8) R. Niewa, Z. Hu, R. Kniep, *Eur. J. Inorg. Chem*., **2003**, 1632.

(9) J. M. Thomas, W. J. Thomas, *Principles and Practice of Heterogeneous Catalysis*, VCH: Weinheim, **1997**, 196.

(10) F. C. Brown, R. Z. Bachrach, A. Bianconi, *Chem. Phys. Lett.*, **1978**, 54, 425.

(11) Y. Xi, C. Reed, Y-K. Lee, S. T. Oyama, *In preparation*.

(12) T. Ressler, Winxas 2.0 Manual.

(13) C. Reed, Y. Xi, Y-K. Lee, S. T. Oyama, *In preparation*.

(14) C. Pelizzi, G. Pelizzi, P. Tarasconi, *J. Chem. Soc. Dalton Trans*., **1985**, 215.

(15) H. Hu, I. E. Wachs, *J. Phys. Chem.*, **1995**, 99, 10911.

(16) J. M. Jehag, H. Hu, X. Gao, I. E. Wachs, *Catal. Today*, **1996**, 28, 335.

(17) L. J. Burcham, L. E. Briand, I. E. Wachs, *Langmiur*, **2001**, 17, 6164.

(18) L. E. Briand, W. E. Farneth, I. E. Wachs, *Catal. Today*, **2000**, 62, 219.

(19) S. T. Oyama, R. Radhakrishman, M. Seman, J. N. Kondo, K. Domen, K. Asakura, *J. Phys. Chem. B*, **2003**, 107, 1845.

(20) W. Li, G. V. Gibbs, S. T. Oyama, *J. Am. Chem. Soc.,* **1998**, 120, 9041.

(21) W. Li, S. T. Oyama, *J. Am. Chem. Soc*., **1998**, 120, 9047.